

Energetics, forces, and quantized conductance in jellium-modeled metallic nanowires

Constantine Yannouleas, Eduard N. Bogachek, and Uzi Landman

School of Physics, Georgia Institute of Technology, Atlanta, Georgia 30332-0430

(Received 6 October 1997)

Energetics and quantized conductance in jellium-modeled nanowires are investigated using the local-density-functional-based shell correction method, extending our previous study of uniform-in-shape wires [C. Yannouleas and U. Landman, *J. Phys. Chem. B* **101**, 5780 (1997)] to wires containing a variable-shaped constricted region. The energetics of the wire (sodium) as a function of the length of the volume-conserving, adiabatically shaped constriction, or equivalently its minimum width, leads to the formation of self-selecting magic wire configurations, i.e., a discrete configurational sequence of enhanced stability, originating from quantization of the electronic spectrum, namely, formation of transverse subbands due to the reduced lateral dimensions of the wire. These subbands are the analogs of shells in finite-size, zero-dimensional fermionic systems, such as metal clusters, atomic nuclei, and ^3He clusters, where magic numbers are known to occur. These variations in the energy result in oscillations in the force required to elongate the wire and are directly correlated with the stepwise variations of the conductance of the nanowire in units of $2e^2/h$. The oscillatory patterns in the energetics and forces, and the correlated stepwise variation in the conductance, are shown, numerically and through a semiclassical analysis, to be dominated by the quantized spectrum of the transverse states at the most narrow part of the constriction in the wire. [S0163-1829(98)01908-0]

I. INTRODUCTION

Understanding the physical origins and systematics underlying the variations of materials properties with size, form of aggregation, and dimensionality is one of the main challenges in modern materials research, and it is of ever increasing importance in the face of the accelerated trend toward miniaturization of electronic and mechanical devices.¹⁻⁴

Interestingly, it has emerged that concepts and methodologies developed in the context of isolated gas-phase clusters and atomic nuclei are often most useful for investigations of finite-size solid-state structures. In particular, it has been shown most recently^{5,6} through first-principles molecular-dynamics simulations that as metallic (sodium) nanowires are stretched to just a few atoms in diameter, the reduced dimensions, increased surface-to-volume ratio, and impoverished atomic environment, lead to the formation of structures, made of the metal atoms in the neck, which can be described in terms of those observed in small gas-phase sodium clusters; hence they were termed^{5,6} supported *cluster-derived structures* (CDS's). The above prediction of the occurrence of "magic-number" CDS's in nanowires, due to characteristics of electronic cohesion and atomic bonding in such structures of reduced dimensions, is directly correlated with the energetics of metal clusters, where magic-number sequences of cluster sizes, shapes, and structural motifs due to electronic and/or geometric shell effects have been long predicted and observed.⁷⁻⁹

These results lead one directly to conclude that other properties of nanowires, derived from their energetics, may be described using methodologies developed previously in the context of clusters. Indeed, in a previous work,¹⁰ we showed that certain aspects of the mechanical response (i.e., elongation force) and electronic transport (e.g., quantized conductance) in metallic nanowires can be analyzed using the local-density-approximation-(LDA-) based shell correc-

tion method (SCM), developed and applied previously in studies of metal clusters.^{8,11} Specifically, we showed that in a jellium-modeled, volume-conserving, and uniform in shape nanowire, variations of the total energy (particularly terms associated with electronic subband corrections) upon elongation of the wire lead to *self-selection* of a sequence of stable "magic" wire configurations (MWC's, specified by a sequence of the wire's radii), with the force required to elongate the wire from one configuration to the next exhibiting an oscillatory behavior. Moreover, we showed that due to the quantized nature of electronic states in such wires, the electronic conductance varies in a quantized stepwise manner (in units of the conductance quantum $g_0=2e^2/h$), correlated with the transitions between MWC's and the above-mentioned force oscillations.

In this paper, we expand our LDA-based treatment to wires of variable shape, which allows for a constricted region. From this investigation, we conclude that the above self-selection principles and the direct correlations between the oscillatory patterns in the energetic stability, forces, and stepwise variations of the quantized conductance maintain for the variable-shaped wire as well, with the finding that underlying these oscillatory patterns and correlations are the contributions from the narrowest region of the wire. Furthermore, this finding is analyzed and corroborated through a semiclassical analysis.

Prior to introducing the model studied in this paper, it is appropriate to briefly describe certain previous theoretical and experimental investigations, which form the background and motivation for this study. Atomistic descriptions, based on realistic interatomic interactions, and/or first-principles modeling and simulations played an essential role in discovering the formation of nanowires,¹² and in predicting and elucidating the microscopic mechanisms underlying their mechanical, spectral, electronic, and transport properties.

These predictions^{12–14} [particularly those pertaining to generation of nanowires through separation of the contact between two material bodies, size-dependent evolution of the wire’s mechanical response to elongation transforming from multiple slips for wider wires to a succession of stress accumulation and fast relief stages leading to a sequence of structural instabilities and order-disorder transformations localized in the neck region when its diameter shrinks to about 15 Å, consequent oscillations of the elongation force and the calculated high value of the resolved yield stress (~ 4 GPa for Au nanowires, which is over an order of magnitude that of the bulk), as well as anticipated electronic quantization effects on transport properties^{12,15}] have been corroborated in a number of experiments using scanning tunneling and force microscopy,^{12,16–21} break junctions,²² and pin-plate techniques^{13,23} at ambient environments, as well as under ultrahigh vacuum and/or cryogenic conditions. Particularly pertinent to our current study are experimental observations of the oscillatory behavior of the elongation forces and the correlations between the changes in the conductance and the force oscillations; see especially the simultaneous measurements of force and conductance in gold nanowires in Ref. 20, where in addition the predicted “ideal” value of the critical yield stress has also been measured (see also Ref. 21).

The LDA-jellium-based model introduced in our previous paper¹⁰ and extended to generalized wire shapes herein, while providing an appropriate solution within the model’s assumptions (see Sec. II), is devoid by construction of atomic crystallographic structure and does not address issues pertaining to nanowire formation methods, atomistic configurations, and mechanical response modes [e.g., plastic deformation mechanisms, interplanar slip, ordering and disordering mechanisms (see detailed descriptions in Refs. 12, 13, and 14, and a discussion of conductance dips in Ref. 18), defects, mechanical reversibility,^{20,13} and roughening of the wires’s morphology during elongation¹⁴], nor does it consider the effects of the above on the electron spectrum, transport properties, and dynamics.⁶ Nevertheless, as shown below, the model offers a useful framework for linking investigations of solid-state structures of reduced dimensions (e.g., nanowires) with methodologies developed in cluster physics, as well as highlighting certain nanowire phenomena of mesoscopic origins and their analogies to clusters.

In this context, we note that several other treatments related to certain of the issues in this paper, but employing free-electron models, have been pursued most recently.^{24,25} In both of these treatments an infinite confining potential on the surface of the wire is assumed and only the contribution from the kinetic energy of the electrons to the total energy is considered, neglecting the exchange-correlation and Hartree terms, and electrostatic interactions due to the positive ionic (jellium) background. A comprehensive discussion of the limitations of such free-electron models in the context of calculations of electronic structure and energetics (e.g., surface energies) of metal surfaces can be found in Ref. 26.

In Sec. II A, we outline the LDA-based shell correction method, describe the jellium model for variable-shaped nanowires, and derive expressions for the energetics of such nanowires (density of states, energy, and force). Numerical results pertaining to energetics, force, and electronic conduc-

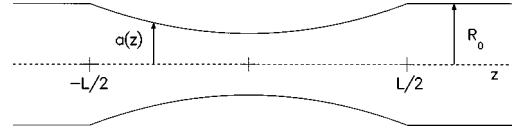


FIG. 1. Schematic drawing of the jellium background of a variable-shaped nanowire. The (cylindrical) symmetry axis of the wire is along the z axis, with a constricted region ($-L/2 \leq z \leq L/2$) described by a dependence of the cross-sectional radii $a(z)$ on z [see Eq. (1)]. $R_0 = a(z = \pm L/2)$ is the radius in the uniform part of the wire outside the constriction.

tance, calculated as a function of elongation for variable-shaped sodium nanowires, are given in Sec. II B, including a discussion on the main finding that the contribution from the narrowest part of the constriction underlies the properties of these quantities and the correlations between them. These correlations between the energetic and transport properties and their dependence on the narrowest part of the nanowire are further analyzed in Sec. III, using a semiclassical treatment. We summarize our results in Sec. IV.

II. DENSITY-FUNCTIONAL DESCRIPTION OF JELLIUM NANOWIRE

A. Theory

1. Shape of constriction

Consider a jellium nanowire with circular symmetry about the axis of the wire (z axis). The wire may contain a constricted region (see Fig. 1), that is, a section of length L where the cross-sectional radius $a(z)$ varies along the axis as

$$a(z) = a_0 + (R_0 - a_0)f(z), \quad -L/2 \leq z \leq L/2, \quad (1)$$

with $f(-z) = f(z)$ (the $z=0$ plane passes through the middle of the wire) and $f(\pm L/2) = 1$. $R_0 = a(\pm L/2)$ is the uniform radius outside the constricted section, and $a_0 \equiv a(0)$. In this paper, we take a parabolic shape $f(z) = (2z/L)^2$ for the description of the constricted region [a wire of uniform cross section throughout corresponds to $f(z) = 1$].

We also assume that elongation of the wire occurs in the constricted region while maintaining its volume constant (this is supported by MD simulations¹²), namely, by requiring that

$$2 \int_0^{L/2} a^2(z) dz = R_0^2 L_0 \quad (2)$$

for given values of R_0 and L_0 [hereafter we will denote the pair of parameters (R_0, L_0) by \mathcal{O} ; we further assume that $R_0 \leq L_0$]. For the parabolic shape assumed in this paper, the smallest cross-sectional radius is determined for any given value of $L_0 \leq L \leq 5L_0$ from Eqs. (1) and (2) as

$$a_0 = \frac{R_0}{4} \left[-1 + \left(30 \frac{L_0}{L} - 5 \right)^{1/2} \right], \quad (3)$$

i.e., $a_0 = R_0$ for $L = L_0$, and $a_0 = 0$ (i.e., breakage of the wire) for $L = 5L_0$.

2. Shell correction method

The shell correction method we employ is based on the LDA theory. In the shell correction method^{8,11,27,28} (SCM), the total LDA energy, $E_T(L, \mathcal{O})$, for any configuration of the wire (specified by L and \mathcal{O}) is separated as

$$E_T(L, \mathcal{O}) = \tilde{E}(L, \mathcal{O}) + \Delta E_{\text{sh}}(L, \mathcal{O}), \quad (4)$$

where $\tilde{E}(L, \mathcal{O})$ varies smoothly as a function of the system size (L) while $\Delta E_{\text{sh}}(L, \mathcal{O})$ varies in an oscillatory manner with L , as a result of the quantization of the electronic states. $\Delta E_{\text{sh}}(L, \mathcal{O})$ is usually called a shell correction in the nuclear^{29,30} and cluster^{8,11} literature; we continue to use here the same terminology with the understanding that the electronic levels in the nanowire form subbands, which are the analog of electronic shells in clusters where the size of the system is usually given by specifying the number of atoms N . The SCM method, which has been shown to yield results in excellent agreement with experiments^{8,27,28} and self-consistent LDA calculations^{8,11} for a number of cluster systems, is equivalent to a Harris functional (E_{Harris}) approximation to the Kohn-Sham LDA with the input density, ρ^{in} , obtained through variational minimization of an extended Thomas-Fermi (ETF) energy functional, $E_{\text{ETF}}[\rho]$.

The Harris functional is given by the following expression:

$$E_{\text{Harris}}[\rho^{\text{in}}] = E_I + \sum_{i=1}^{\text{occ}} \epsilon_i^{\text{out}} - \int \left\{ \frac{1}{2} V_H[\rho^{\text{in}}(\mathbf{r})] + V_{\text{xc}}[\rho^{\text{in}}(\mathbf{r})] \right\} \rho^{\text{in}}(\mathbf{r}) d\mathbf{r} + \int \mathcal{E}_{\text{xc}}[\rho^{\text{in}}(\mathbf{r})] d\mathbf{r}, \quad (5)$$

where V_H is the Hartree (electronic) repulsive potential, E_I is the repulsive electrostatic energy of the ions, and $E_{\text{xc}} \equiv \int \mathcal{E}_{\text{xc}}[\rho] d\mathbf{r}$ is the exchange-correlation (xc) functional³¹ (the corresponding xc potential is given as $V_{\text{xc}}(\mathbf{r}) \equiv \delta E_{\text{xc}}[\rho] / \delta \rho(\mathbf{r})$). ϵ_i^{out} are the eigenvalues (non-self-consistent) of the single-particle Hamiltonian,

$$\hat{H} = -\frac{\hbar^2}{2m_e} \nabla^2 + V_{\text{in}}, \quad (6)$$

with the mean-field potential given by

$$V_{\text{in}}[\rho^{\text{in}}(\mathbf{r})] = V_H[\rho^{\text{in}}(\mathbf{r})] + V_{\text{xc}}[\rho^{\text{in}}(\mathbf{r})] + V_I(\mathbf{r}), \quad (7)$$

$V_I(\mathbf{r})$ being the attractive potential between the electrons and ions.

In electronic structure calculations where the corpuscular nature of the ions is included (i.e., all-electron or pseudopotential calculations), ρ^{in} may be taken as a superposition of atomic-site densities. In the case of jellium calculations, we have shown^{8,11} that an accurate approximation to the KS-LDA total energy is obtained by using the Harris functional with the input density ρ^{in} in Eq. (5) evaluated from a variational extended-Thomas-Fermi (ETF)-LDA calculation.

The ETF-LDA energy functional $E_{\text{ETF}}[\rho]$ is obtained by replacing the kinetic energy term $T[\rho]$ in the usual LDA functional, namely, in the expression

$$E_{\text{LDA}}[\rho] = T[\rho] + \int \left\{ \frac{1}{2} V_H[\rho(\mathbf{r})] + V_I(\mathbf{r}) \right\} \rho(\mathbf{r}) d\mathbf{r} + \int \mathcal{E}_{\text{xc}}[\rho(\mathbf{r})] d\mathbf{r} + E_I, \quad (8)$$

by the ETF kinetic energy, given to the fourth-order gradients as follows:³²

$$\begin{aligned} \frac{2m_e}{\hbar^2} T_{\text{ETF}}[\rho] &= \frac{2m_e}{\hbar^2} \int t_{\text{ETF}}[\rho] d\mathbf{r} = \int \left\{ \frac{3}{5} (3\pi^2)^{2/3} \rho^{5/3} + \frac{1}{36} \frac{(\nabla \rho)^2}{\rho} + \frac{1}{270} (3\pi^2)^{-2/3} \rho^{1/3} \right. \\ &\quad \left. \times \left[\frac{1}{3} \left(\frac{\nabla \rho}{\rho} \right)^4 - \frac{9}{8} \left(\frac{\nabla \rho}{\rho} \right)^2 \frac{\Delta \rho}{\rho} + \left(\frac{\Delta \rho}{\rho} \right)^2 \right] \right\} d\mathbf{r}. \end{aligned} \quad (9)$$

The optimal ETF-LDA total energy is then obtained by minimization of $E_{\text{ETF}}[\rho]$ with respect to the density. In our calculations, we use for the trial densities parametrized profiles $\rho(\mathbf{r}; \{\gamma_i\})$ with $\{\gamma_i\}$ as variational parameters (the ETF-LDA optimal density is denoted as $\tilde{\rho}$). The single-particle eigenvalues $\{\epsilon_i^{\text{out}}\}$ in Eq. (5) are obtained then as the solutions to the single-particle Hamiltonian of Eq. (6) with V_{in} replaced by V_{ETF} [given by Eq. (7) with $\rho^{\text{in}}(\mathbf{r})$ replaced by $\tilde{\rho}(\mathbf{r})$]. Hereafter, these single-particle eigenvalues will be denoted by $\{\tilde{\epsilon}_i\}$.

In our approach, the smooth contribution in the separation (4) of the total energy is given by $E_{\text{ETF}}[\tilde{\rho}]$, while the shell correction ΔE_{sh} is simply the difference

$$\Delta E_{\text{sh}} = E_{\text{Harris}}[\tilde{\rho}] - E_{\text{ETF}}[\tilde{\rho}]$$

$$= \sum_{i=1}^{\text{occ}} \tilde{\epsilon}_i - \int \tilde{\rho}(\mathbf{r}) V_{\text{ETF}}(\mathbf{r}) d\mathbf{r} - T_{\text{ETF}}[\tilde{\rho}]. \quad (10)$$

3. Adiabatic assumption

The volume density of the positive background is given by $\rho_v^+ = 3/(4\pi r_s^3)$, where r_s is the Wigner-Seitz radius characteristic to the material, and thus the number of positive charges in the constriction is

$$N^+(\mathcal{O}) = 3R_0^2 L_0 / (4r_s^3). \quad (11)$$

Since the nanowire contains a constricted region of variable cross-sectional radius $a(z)$ [see Eq. (1)], we define a linear (i.e., density per unit length of the nanowire) back-

ground density $\rho_l^+(z; L, \mathcal{O}) = 3a^2(z)/(4r_s^3)$, which when integrated over the total length of the wire yields $N^+(\mathcal{O})$ [see Eq. (11)]. Correspondingly, the variational electronic volume density $\tilde{\rho}(\mathbf{x}; L, \mathcal{O}) \equiv \tilde{\rho}(r, z; L, \mathcal{O})$, and in our calculations it takes the form

$$\tilde{\rho}(r, z; L, \mathcal{O}) = \frac{\tilde{\rho}_0(z)}{[1 + \exp\{[r - r_0(z)]/\alpha(z)\}]^{\gamma(z)}}, \quad (12)$$

with $\tilde{\rho}_0(z)$, $\alpha(z)$, and $\gamma(z)$ as z -dependent variational parameters. In the ETF calculation, $\tilde{\rho}$ is determined variationally at a given z as the one associated with a uniform cylinder of radius $a(z)$ (adiabatic assumption), under the normalization condition for local charge neutrality, namely, $2\pi \int dr [r \tilde{\rho}(r, z; L, \mathcal{O})] = \rho_l^+(z; L, \mathcal{O})$ [which fixes the fourth parameter $r_0(z)$ in Eq. (12)]. The optimized $\tilde{\rho}$ allows then calculation of the smooth contribution for any length of the constriction, $\tilde{E}(L, \mathcal{O}) \equiv E_{\text{ETF}}(L, \mathcal{O})$ in Eq. (4).

The calculation of the shell-correction term, $\Delta E_{\text{sh}}(L, \mathcal{O})$, in Eq. (4) proceeds by evaluating first the density of states in the nanowire. Assuming an adiabatic separation of the ‘‘fast’’ transverse and the ‘‘slow’’ longitudinal variables,^{15,33,34} the electronic wave functions in the classically allowed regions may be written as

$$\Psi_{nm\epsilon}(r, \phi, z; L, \mathcal{O}) \propto \psi_{nm}(r; z, L, \mathcal{O}) e^{im\phi} e^{if^z dz' k_{\perp}^{nm}(z'; \epsilon, L, \mathcal{O})}, \quad (13)$$

where k_{\perp}^{nm} is the local wave number along the axial (z) direction of the nanowire

$$k_{\perp}^{nm}(z, \epsilon; L, \mathcal{O}) = \left[\frac{2m_e}{\hbar^2} [\epsilon - \tilde{\epsilon}_{nm}(z; L, \mathcal{O})] \right]^{1/2}, \quad (14)$$

and $\tilde{\epsilon}_{nm}$ is the (transverse) local eigenvalue spectrum at z . To calculate this spectrum for a wire of a configuration specified by (L, \mathcal{O}) for any value of z , the eigenvalues of a cylindrical wire with a (uniform) radius $a(z)$ are calculated from the two-dimensional Schrödinger equation

$$\begin{aligned} & -\frac{\hbar^2}{2m_e} \left[\frac{d^2}{dr^2} + \frac{1}{r} \frac{d}{dr} - \frac{m^2}{r^2} \right] \psi + V_{\text{ETF}}(r; z, L, \mathcal{O}) \psi \\ & = \tilde{\epsilon}_{nm}(z, L, \mathcal{O}) \psi. \end{aligned} \quad (15)$$

The linear (per unit length), one-dimensional density of states at z , $D_l(z, \epsilon; L, \mathcal{O})$, is given by

$$D_l(z, \epsilon; L, \mathcal{O}) = \frac{2}{\pi} \sum_{nm} \frac{\partial k_{\perp}^{nm}(z, \epsilon; L, \mathcal{O})}{\partial \epsilon} \Theta[\epsilon - \tilde{\epsilon}_{nm}(z; L, \mathcal{O})], \quad (16)$$

where spin degeneracy has been included, and Θ is the Heaviside step function.

From Eq. (14), we obtain

$$\begin{aligned} D_l(z, \epsilon; L, \mathcal{O}) &= \left(\frac{2m_e}{\pi^2 \hbar^2} \right)^{1/2} \sum_{nm} [\epsilon - \tilde{\epsilon}_{nm}(z; L, \mathcal{O})]^{-1/2} \\ &\quad \times \Theta[\epsilon - \tilde{\epsilon}_{nm}(z; L, \mathcal{O})]. \end{aligned} \quad (17)$$

We may now define an integrated density of states in the constriction

$$D(\epsilon; L, \mathcal{O}) = \int_{-L/2}^{L/2} dz D_l(z, \epsilon; L, \mathcal{O}). \quad (18)$$

The total number of states up to energy ϵ in the constricted region of the wire is given by

$$\begin{aligned} N^-(\epsilon; L, \mathcal{O}) &= \int_0^{\epsilon} d\epsilon' D(\epsilon'; L, \mathcal{O}) \\ &= \frac{2}{\pi} \int_{-L/2}^{L/2} dz \sum_{nm} \sqrt{\frac{2m_e}{\hbar^2} [\epsilon - \tilde{\epsilon}_{nm}(z; L, \mathcal{O})]} \\ &\quad \times \Theta[\epsilon - \tilde{\epsilon}_{nm}(z; L, \mathcal{O})]. \end{aligned} \quad (19)$$

Since the total number of electrons in the constricted region is $N^+(\mathcal{O})$ [see Eq. (11)], the Fermi energy, $\epsilon_F(L, \mathcal{O})$, for a wire with a configuration specified by (L, \mathcal{O}) is given from Eq. (19), i.e.,

$$N^-(\epsilon_F; L, \mathcal{O}) = N^+(\mathcal{O}). \quad (20)$$

Using the above and Eq. (10), the shell-correction term,

$$\Delta E_{\text{sh}}(L, \mathcal{O}) \equiv E_{\text{Harris}}[\tilde{\rho}; L, \mathcal{O}] - E_{\text{ETF}}[\tilde{\rho}; L, \mathcal{O}], \quad (21)$$

may be calculated as

$$\begin{aligned} \Delta E_{\text{sh}}(L, \mathcal{O}) &= \int_0^{\epsilon_F(L, \mathcal{O})} d\epsilon [\epsilon D(\epsilon; L, \mathcal{O})] - 2\pi \int_{-L/2}^{L/2} dz \int_0^{\infty} dr r \tilde{\rho}(r, z; L, \mathcal{O}) V_{\text{ETF}}(r, z; L, \mathcal{O}) \\ &\quad - 2\pi \int_{-L/2}^{L/2} dz \int_0^{\infty} dr r t_{\text{ETF}}[\tilde{\rho}(r, z; L, \mathcal{O})], \end{aligned} \quad (22)$$

where V_{ETF} is the ETF potential (Hartree, exchange-correlation, and electron attraction to the positive background) and t_{ETF} is the volume density of the ETF kinetic-energy functional [see Eq. (9)].

In actual calculations, we invert the order of integration in the first term of Eq. (22), which then takes the form

$$\frac{2}{3\pi} \int_{-L/2}^{L/2} dz \sum_{nm} [\epsilon_F + 2\tilde{\epsilon}_{nm}(z;L,\mathcal{O})] \sqrt{\frac{2m_e}{\hbar^2} [\epsilon_F - \tilde{\epsilon}_{nm}(z;L,\mathcal{O})]} \Theta[\epsilon_F - \tilde{\epsilon}_{nm}(z;L,\mathcal{O})]. \quad (23)$$

Note that Eq. (20) implies a common Fermi level for the whole constriction for a given L (i.e., ϵ_F is not a local property). Therefore, Eq. (23) is not equivalent to integration of the corresponding uniform wire result derived by us in Ref. 10 over the z coordinate, since there ϵ_F varies with the wire's cross-sectional radius.

Having calculated the smooth and shell-correction contributions to the total energy, as a function of L , the total elongation force may be evaluated as the derivative of the total energy with respect to L , i.e., $F_T = -dE_T/dL$, and the contributions to it from the smooth and shell-correction terms are given by $\tilde{F} = -d\tilde{E}/dL$, and $\Delta F_{\text{sh}} = -d\Delta E_{\text{sh}}/dL$.

B. Results

In this section, we report results for the elongation of a sodium nanowire ($r_s = 4$ a.u.), starting with an initial cylindrical constriction of length $L_0 = 80$ a.u. and radius $R_0 = 25$ a.u.

In Fig. 2, we show electronic-potential profiles, $V_{\text{ETF}}[r; a(z), L, \mathcal{O}]$, for a particular constriction with $\Delta L/L_0 = 1.125$ ($\Delta L = L - L_0$). We display here the potential profiles calculated at the narrowest part of the constriction [$a_0 \equiv a(0) = 12.62$ a.u.] and at its end [i.e., at $a(L/2) = R_0$] (in this paper, all the subsequent numerical results we will dis-

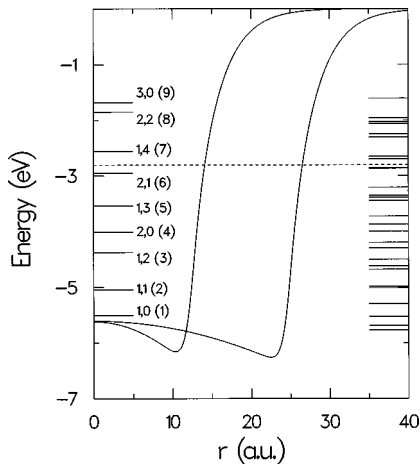


FIG. 2. Potential profiles at the narrowest ($z=0$; left curve) and end points ($z=\pm L/2$; right curve) of a constriction with an elongation $\Delta L/L_0 = 1.125$ (whose \mathcal{O} parameters are $L_0 = 80$ a.u. and $R_0 = 25$ a.u.). The local transverse-mode spectra, $\tilde{\epsilon}_{nm}$, associated with these two profiles are also displayed along the left and right y axes. The dashed line indicates the Fermi level. For the ($z=0$) profile, the spectrum is labeled with the corresponding n, m local transverse eigenvalues (n denotes the number of radial nodes plus one, and m denotes the azimuthal angular-momentum quantum number). The same spectrum is numbered sequentially (in parentheses) to facilitate comparison between the location of the energy levels and the numbered peaks in the density of states given in the lower curve in Fig. 3(a). Energies in units of eV, and lengths in a.u.

cuss relate to constrictions with the same set of \mathcal{O} parameters, namely, $L_0 = 80$ a.u. and $R_0 = 25$ a.u.). We found that for other values of z (i.e., for $0 < |z| < L/2$), the potential assumes profiles intermediate between the two profiles shown here, namely, the depth of the potential well remains practically unaltered, while its width follows the enlargement of the jellium-background radius $a(z)$, from a_0 to $a(L/2)$. From the three components, V_H , V_I , and V_{xc} , which contribute to the total V_{ETF} [see Eq. (7)], we found that for all these potential profiles, calculated for different values of z along the constriction, the xc contribution is the dominant one, amounting to approximately -5.4 eV, while the total electrostatic contribution, $V_H + V_I$, is much smaller, resulting in a characteristic “winebottle” profile familiar from LDA studies of spherical clusters.³⁵

Figure 2 also displays the transverse local eigenvalues $\tilde{\epsilon}_{nm}$ associated with the two potential profiles. Naturally, a wider potential profile yields a larger number of such eigenvalues below the Fermi level.

To illustrate the nature of the electronic spectrum in the nanowires, and its dependencies on the characteristics of the wire, i.e., shape and length, we show in Fig. 3(a) densities of states, $D(\epsilon; L, \mathcal{O})$, calculated for a variable-shaped wire for two wire lengths (and consequently two minimal cross-sectional radii of the constricted region). The density of states for a uniform wire with a radius equal to that of the unconstricted region of the variable-shaped ones [shown in Fig. 3(a)] is displayed in Fig. 3(b).

Two “classes” of features are noted for the variable-shaped wires: (i) those associated with the narrowest constricted region (marked by numbers) whose radius a_0 varies upon elongation, and (ii) those associated with the maximal radius of the wire (and with the unconstricted part of the wire), which remains constant throughout the elongation of the wire. Identification of the latter class of features (several of which are marked by arrows) is facilitated through comparison with the density of states for the corresponding uniform wire [Fig. 3(b)]. We observe here that, for the broader (and thus shorter) wire [lower curve in Fig. 3(a)], six of the features (peaks) in the density of states coming from the spectrum of transverse energy levels at the narrowest region of the constriction are located below the Fermi level ϵ_F [all the peaks in the density of states occur at the energies of the transverse levels; e.g., compare the location of the peaks in the density of states in Fig. 3(a) with the corresponding spectrum on the left side of Fig. 2].

On the other hand, for the much narrower (and thus longer) constricted wire, only one of these peaks is below ϵ_F [see upper curve in Fig. 3(a)]. When plotting the density of states at ϵ_F versus the elongation (or equivalently the minimal radius of the constricted region), these variations lead to an oscillatory pattern, as peaks in the density of states are shifted above the Fermi level, one after the other as the wire is being elongated. These variations are also portrayed in the energetics of the wire (shown in Fig. 4), and in the stepwise behavior of the quantized conductance through the wire versus length (see Fig. 5 below).

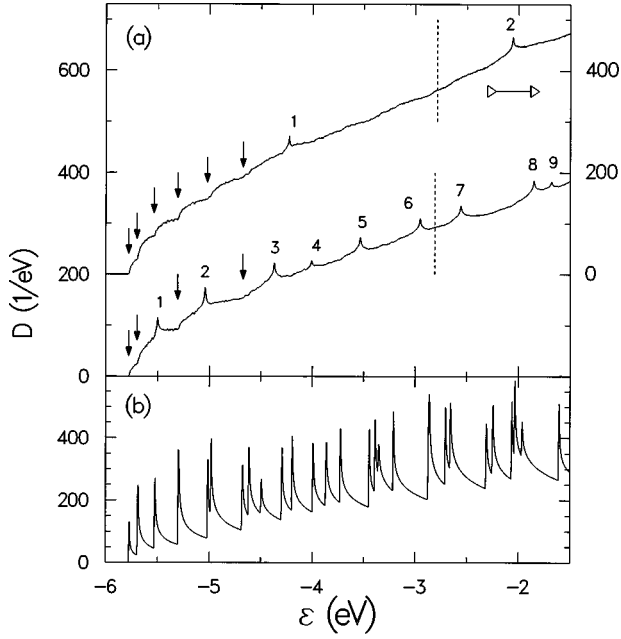


FIG. 3. Densities of states for (a) two configurations of the variable-shaped wire, one (lower curve) with elongation $\Delta L/L_0 = 1.125$ and narrowest radius $a_0 = 12.62$ a.u. (potential profiles and local transverse spectra for this case are displayed in Fig. 2), and the other with elongation $\Delta L/L_0 = 2.75$ and narrowest radius $a_0 = 4.57$ a.u. (upper curve whose y axis is shown on the right). (b) a uniform-in-shape wire with $\Delta L/L_0 = 0$ and $a_0 = R_0 = 25$ a.u. For all cases, $L_0 = 80$ a.u. and $R_0 = 25$ a.u. The vertical dashed lines denote the corresponding Fermi levels. The Fermi level of the constrictions, which for the uniform-in-shape wire is -2.82 eV, varies only by 0.05 eV for all the elongations down to the breakage point. In (a) the numbered peaks correspond to the locations of the transverse energy levels in the narrowest part of the constriction [e.g., compare the lower curve in (a) with the spectrum shown on the left axis of Fig. 2]. The arrows indicate the locations of some of the transverse energy levels at the end points of the constriction, coinciding with corresponding peaks in the spectrum of the uniform-in-shape wire shown in (b).

From Fig. 4, we observe that the magnitude of the smooth ETF contribution \tilde{E} to the total energy E_T of the wire is dominant, with the shell-correction contribution, ΔE_{sh} , exhibiting an oscillatory pattern, with local minima at a set of wire lengths (and correspondingly a set of minimal cross-sectional radii), which we term ‘‘magic wire configurations’’ (MWC’s), i.e., wire configurations with enhanced energetic stability. When added to the smooth contribution, these shell-correction features lead to local minima of the total energy toward the end of the elongation (and consequently, narrowing) process, while for thicker wires (i.e., $\Delta L/L_0 \leq 2.5$ in Fig. 4) they are expressed as inflection points of the total energy (in this context, see the total-force curve F_T in Fig. 5, where the local minimum in E_T corresponds to the point with $F_T = 0$ marked by an arrow).

We note here that the occurrence of local minima in the total energy results from a balance between ΔE_{sh} and \tilde{E} , with the latter increasing (that is acquiring less negative values) as the constriction elongates due to the increasing contribution from the surface of the constriction. Comparison of the magnitudes of the shell corrections in a variable-shaped

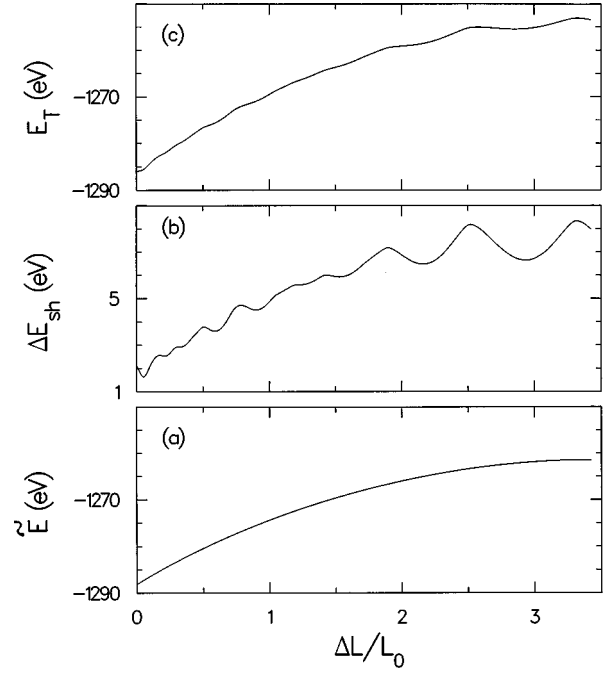


FIG. 4. Energies (in eV units) of a variable-shaped sodium nanowire, plotted vs the relative elongation $\Delta L/L_0$. The initial parameters \mathcal{O} are $L_0 = 80$ a.u. and $R_0 = 25$ a.u. The smooth, ETF contribution (\tilde{E}), the shell correction (ΔE_{sh}), and the total energy (E_T) are displayed in (a), (b), and (c), respectively.

wire and in a uniform one [i.e., one with $f(z) \equiv 1$ in Eq. (1), whose case was discussed in Ref. 10] shows that the amplitudes of the oscillations in the latter case are much larger (over an order of magnitude). The reason for this difference is that in the constant-radius wire the quantization into the transverse subbands is uniform along the wire, while in the variable-shaped case the subband spectrum is different in various parts of the constriction. While the oscillatory pattern is dominated by the spectrum at the narrowest region (see also Sec. III below), the amplitudes are influenced by the transverse-mode spectra from other parts of the constriction. Consequently, the number of local minima in the total energy E_T (and thus the number of wire configurations, i.e., lengths, for which the total force F_T vanishes) is larger for a uniform wire than for a variable-shaped one. Additionally, we suggest that for materials with relatively smaller surface energies a larger number of local minima may occur.

From the total energy, and the smooth and shell-correction contributions to it, we obtain the total ‘‘elongation force’’ (EF) F_T and the corresponding components of it, \tilde{F} and ΔF_{sh} . These results are displayed in Fig. 5, along with the conductance of the wire evaluated, in the adiabatic approximation (i.e., no mode mixing³³) and neglecting tunneling effects (assuming unit transmission coefficients for all the conducting modes), using the Landauer expression^{36,37}

$$G(L, \mathcal{O}) = g_0 \sum_{nm} \Theta[\epsilon_F - \tilde{\epsilon}_{nm}(z=0; L, \mathcal{O})], \quad (24)$$

where $g_0 = 2e^2/h$, and the spectrum of the transverse modes is evaluated (for each constriction length) at the narrowest part of the constriction, $z=0$. Tunneling contributions (see,

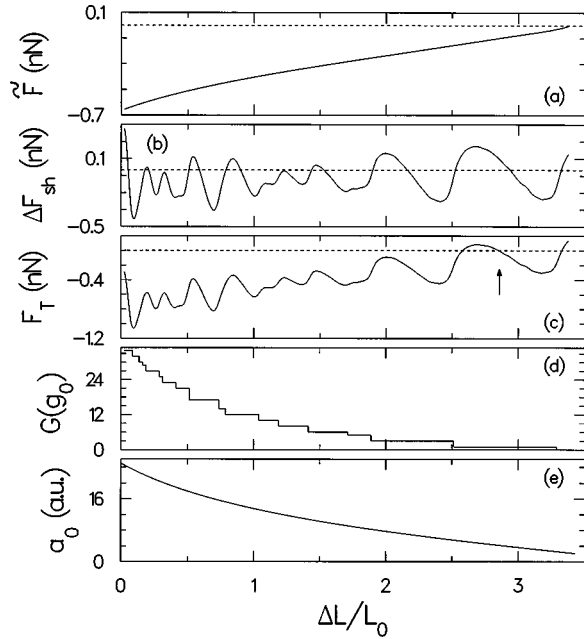


FIG. 5. (a)–(c) The smooth, ETF contribution to the force (\bar{F}), shell-correction force (ΔF_{sh}), and total force (F_T), corresponding to the energies shown in Figs. 4(a)–4(c), plotted vs the relative elongation $\Delta L/L_0$. The arrow in (c) indicates the point $F_T=0$ corresponding to the local minimum in the total energy shown in Fig. 4(c). The dashed lines indicate the zeroes of the y axes. Forces in units of nanonewtons. (d) The conductance G for the variable-shaped wire in units of $g_0 = 2e^2/h$, plotted vs $\Delta L/L_0$, evaluated as described by Eq. (24). (e) The variation of the cross-sectional radius (in a.u.) of the narrowest part of the constriction, plotted vs $\Delta L/L_0$ [see Eq. (3), with $L_0 = 80$ a.u. and $R_0 = 25$ a.u.].

e.g., Ref. 38), mode-mixing, and nonadiabaticity may affect the sharpness of the conductance steps, and/or introduce some interference-related features, particularly near the transitions between the conductance plateaus. These effects, which can be included in more elaborate evaluations of the conductance,^{39–41} do not modify the conclusions of our study.

Also included in this figure is a plot describing the variation of the minimal cross-sectional radius a_0 with the length of the constriction [see Eq. (3)].

As evident from Fig. 5, the oscillations in the force resulting from the shell-correction contributions are prominent. In ΔF_{sh} , we observe that the locations of the zeroes of the force situated at the right of the force maxima occur for values of $\Delta L/L_0$ which coincide with the locations of local minima in the shell-correction contribution to the energy of the wire (i.e., for a sequence of minimal cross-sectional radii corresponding to MWC's). In the total force F_T only one of these points (where $F_T=0$) remains [i.e., the one corresponding to the local minimum in the total energy towards the end of the elongation process (see Fig. 4)], for the reasons discussed above in connection with the energetics of the wire. Nevertheless, the oscillations in the total force correlate well with those in the total energy of the wire, which as discussed above originate from the subband spectrum at the narrowest part of the constriction (see also Sec. III). Also, the locations of the local maxima in the total force correlate with the stepwise variations in the conductance signifying

the sequential decrease in the number of transverse subbands (calculated at the narrowest section of the wire) below ϵ_F (i.e., conducting channels) as the constricted part of the wire elongates (and thus narrows). Additionally, we note that the magnitude of the total force is comparable to measured ones (i.e., in the nanonewton range). The magnitude of the total force in sodium nanowires (not measured to date) is expected to be smaller than that found for gold nanowires,^{20,21} due mainly to differences in the electron densities and surface energies of the materials.

III. SEMICLASSICAL ANALYSIS

As discussed above, the total energy of the wire is characterized by local minima and inflection points occurring for a set of wire lengths, or equivalently a set of minimal cross-sectional radii of the constriction, and are reflected in the oscillatory patterns of the elongation force. These features correspond to the oscillatory shell-correction contributions and originate from the spectrum of transverse modes at the narrowest part of the constriction. Moreover, these patterns correlate with the locations of the quantized conductance steps, which are determined by the transverse-mode spectrum at the narrowest region (i.e., the number of conducting modes below ϵ_F , and their degeneracies).

To further investigate the origins of these correlations, we present in this section a semiclassical analysis of the density of states, energetics, forces, and conductance in a free-electron nanowire modeled via an infinite confining potential on the surface of the wire. As in the above (see Fig. 1), we model the constricted region of the wire as a section with a slowly (adiabatically) varying shape. Dividing the constriction into thin cylindrical slices, the solution of the Schrödinger equation for each slice is of the form

$$\psi = \mathcal{A} J_m(\kappa r) e^{im\phi} e^{ip_{\perp}z}, \quad (25)$$

where \mathcal{A} is a normalization constant, p_{\perp} is the electron momentum along the axis of the wire, $J_m(\kappa r)$ is the Bessel function of order m , and $\kappa = (2m_e \epsilon - p_{\perp}^2)^{1/2}/\hbar$.

Consider first a uniform cylindrical wire with a constant cross-sectional radius a . With the infinite wall boundary condition assumed here, the single-particle electronic energy levels in the wire are expressed in terms of the roots of the Bessel functions, γ_{nm} , as

$$\epsilon_{nm,p_{\perp}} = \frac{\hbar^2 \gamma_{nm}^2}{2m_e a^2} + \frac{p_{\perp}^2}{2m_e}. \quad (26)$$

Here we remark that in the semiclassical approximation the electron performs a complicated trajectory inside the wire. All the semiclassical trajectories are tangent to the caustic surfaces of a set of concentric cylinders inside the wire.⁴² Quantization of the electronic states leads to selection of only a certain subset of trajectories associated with a certain set of radii r_m of the caustic surfaces, corresponding to allowed values of the azimuthal quantum numbers, m , i.e., $\kappa r_m = m$; this description is closely related to the semiclassical periodic orbit theory.⁴³ In the course of developing semiclassical methods, Keller and Rubinow⁴² have demonstrated

that the Debye asymptotic expansion⁴⁴ of the Bessel functions ($1 \ll m < \kappa r$) provides an accurate approximation to the eigenfunction $J_m(\kappa r)$, i.e.,

$$J_m(r) \sim \left(\frac{2}{\pi}\right)^{1/2} (\kappa^2 r^2 - m^2)^{-1/4} \sin\left[(\kappa^2 r^2 - m^2)^{1/2} - \text{marccos}\left(\frac{m}{\kappa r}\right) + \frac{\pi}{4}\right]. \quad (27)$$

This approximation is valid in the region between the caustic cylindrical surface and the boundary surface of the wire; in the region inside the caustic surface ($m > \kappa r$) the solution decays exponentially. In this approximation, the equation for the asymptotic values of the Bessel-function zeroes has the form

$$(\gamma_{nm}^2 - m^2)^{1/2} - \text{marccos}\left(\frac{m}{\gamma_{nm}}\right) = \pi\left(n - \frac{1}{4}\right). \quad (28)$$

First we calculate the density of states whose evaluation involves, after integration over p_\perp , double sums over the quantum numbers n and m ; $n = 1, 2, \dots$, $m = 0, \pm 1, \pm 2, \dots$ [see Eq. (17)]. Applying sequentially the Poisson summation formula to both sums and separating the oscillatory terms (note that in our semiclassical approximation $\kappa a \gg 1$) in complete analogy with Refs. 45 and 46, we obtain for the density of states (per unit length),

$$D_l^{\text{osc}}(\epsilon) = \frac{2}{\pi a \epsilon_a} \sum_{M=2}^{\infty} \sum_{Q=1}^{M/2} \frac{1}{M} \sin\left(\frac{\pi Q}{M}\right) \times \cos\left[2MKa \sin\left(\frac{\pi Q}{M}\right) + \frac{\pi M}{2}\right] + \frac{2\sqrt{2}}{\pi a \epsilon_a^{3/4} \epsilon^{1/4}} \sum_{M=1}^{\infty} \frac{1}{M^{1/2}} \sin\left[2\pi MKa + \frac{\pi}{4}\right], \quad (29)$$

where $\epsilon_a = \hbar^2/(2m_e a^2)$, and K is the electron wave vector. The two terms in Eq. (29) correspond to the contribution from the point where the phase is stationary and from the end points in the sum (integral) over m (see discussion in Ref. 46). While the second oscillatory term in Eq. (29) has a smaller amplitude than the first one [by a factor of $(Ka)^{1/2}$], it corresponds to an important class of electronic states, with $m \approx Ka$, localized near the surface of the wire (the so-called whispering gallery states⁴⁶).

Until now we discussed a uniform wire with a constant cross-sectional radius. In a wire with a variable shape, the cross-sectional radii depend on z , as discussed in connection with Eq. (1). Substituting the z dependence of the radii in Eq. (29), i.e., replacing a by $a(z)$, we need to perform an integration over z [see Eq. (18)]. This integration involves evaluation of integrals of the form

$$I = \text{Re} \int_{-L/2}^{L/2} g(z) e^{i\alpha Ka(z)} dz, \quad (30)$$

where for the first term in Eq. (29) $g(z) = a(z)$ and $\alpha = 2M \sin(\pi Q/M)$, and for the second one $g(z) = \sqrt{a(z)}$ and $\alpha = 2\pi M$. The fast oscillatory character of the exponential factor [i.e., $Ka(z) \gg 1$ for all z] relative to the slow variation of $g(z)$ allows us to use the standard stationary phase method,⁴⁷ obtaining

$$I \approx \left[\frac{2\pi}{\alpha Ka''(0)}\right]^{1/2} g(0) \text{Re}\{\exp[i\alpha Ka(0) + i\pi/4]\} + \frac{2}{\alpha Ka'(L/2)} g(L/2) \text{Re}\{-i \exp[i\alpha Ka(L/2)]\}, \quad (31)$$

where $z=0$ is the stationary (extremum) point, the second term is the contribution from the end-points of the integral, and primes denote differentiation with respect to z . Using the above, and after simple algebraic manipulations, we obtain for the oscillatory part of the density of states,

$$D^{\text{osc}}(\epsilon) = \frac{2}{\pi} \sum_{M=2}^{\infty} \sum_{Q=1}^{M/2} \left\{ \frac{1}{M^{3/2}} \left[\sin\left(\frac{\pi Q}{M}\right) \right]^{1/2} \left[\frac{\pi}{Ka''(0)} \right]^{1/2} \frac{2m_e a(0)}{\hbar^2} \cos\left[2MKa(0) \sin\left(\frac{\pi Q}{M}\right) + \frac{\pi}{2}\left(M + \frac{1}{2}\right)\right] + \frac{1}{M^2} \frac{2m_e a(L/2)}{\hbar^2 Ka'(L/2)} \sin\left[2MKa(L/2) \sin\left(\frac{\pi Q}{M}\right) + \frac{\pi M}{2}\right] \right\} + \frac{2\sqrt{2}}{\pi \epsilon^{1/4}} \sum_{M=1}^{\infty} \left\{ \frac{1}{M} \left[\frac{1}{Ka''(0)} \right]^{1/2} \frac{1}{a(0)} \times \left(\frac{2m_e a^2(0)}{\hbar^2} \right)^{3/4} \cos[2\pi MKa(0)] - \frac{1}{\pi M^{3/2}} \frac{1}{Ka'(L/2)a(L/2)} \left(\frac{2m_e a^2(L/2)}{\hbar^2} \right)^{3/4} \cos\left[2\pi MKa(L/2) + \frac{\pi}{4}\right] \right\}. \quad (32)$$

The density of states of the wire contains oscillatory contributions from the narrowest cross section of the wire [first and third terms in Eq. (32)] and from the wire's-end cross sections (second and fourth terms). The amplitudes of the latter oscillations are smaller.

Having obtained the expression for the oscillatory part of the density of states, we can calculate now the semiclassical approximation to the grand-canonical thermodynamic potential Ω [see the Appendix; at zero temperature, $\Omega = \int (\epsilon - \epsilon_F) D(\epsilon) d\epsilon$]. Restricting ourselves for brevity to the largest contribution [that is, to the first term in Eq. (32) corresponding to the main contribution from the narrowest part of the wire], we get for the oscillatory part of Ω ,

$$\Omega^{\text{osc}} \approx \frac{2\epsilon_F}{\sqrt{\pi k_F a''(0) a(0)}} \sum_{M=2}^{\infty} \sum_{Q=1}^{M/2} \frac{1}{M^{7/2}} \sin^{-3/2}(\pi Q/M) \cos \left[2M k_F a(0) \sin(\pi Q/M) + \frac{\pi}{2} \left(M + \frac{1}{2} \right) \right]. \quad (33)$$

From this expression, the oscillating part of the force as a function of the length of the constricted region [i.e., $a(0)$ in general depends on L , see e.g., Eq. (3)] is given by

$$F^{\text{osc}}(L) = - \frac{\partial \Omega^{\text{osc}}}{\partial a(0)} \frac{\partial a(0)}{\partial L}, \quad (34)$$

which upon substitution of Eq. (33) yields

$$F^{\text{osc}}(L) \approx \frac{4\epsilon_F k_F^{1/2} [\partial a(0)/\partial L]}{\sqrt{\pi a''(0) a(0)}} \sum_{M=2}^{\infty} \sum_{Q=1}^{M/2} \frac{1}{M^{5/2}} \sin^{-1/2}(\pi Q/M) \cos \left[2M k_F a(0) \sin(\pi Q/M) + \frac{\pi}{2} \left(M - \frac{1}{2} \right) \right]. \quad (35)$$

The expression for the conductance of the wire following the Landauer formula involves evaluation of the number of transverse states in the narrowest part of the wire. Following Ref. 48,

$$G \approx \left(\frac{2e^2}{h} \right) \frac{[k_F a(0)]^2}{4} \left\{ 1 - \frac{2}{k_F a(0)} + \frac{8}{\sqrt{\pi}} \frac{1}{[k_F a(0)]^{3/2}} \sum_{M=2}^{\infty} \sum_{Q=1}^{M/2} \frac{1}{M^{3/2}} \sin^{1/2}(\pi Q/M) \right. \\ \left. \times \cos \left[2M k_F a(0) \sin(\pi Q/M) + \frac{\pi}{2} \left(M - \frac{1}{2} \right) \right] \right\}, \quad (36)$$

which can be expressed as a function of the length of the constriction [see e.g., Eq. (3); we remark here that our semiclassical treatment is valid for any adiabatic wire shape].

The nonoscillating contribution (coming from the first two terms in curly brackets) describes the Sharvin⁴⁹ conductance of the constriction and the Weyl⁵⁰ semiclassical corrections, and the third term describes conductance quantum oscillations as a function of $a(0)$. From a comparison of the expression for the oscillatory contribution to the force [Eq. (35)] with the oscillatory contribution to the conductance [Eq. (36)], the direct correlation between the two is immediately evident, and both depend on the spectrum of transverse modes (conducting channels) at the narrowest part of the wire. This is in agreement with the results shown in Fig. 5 obtained through the LDA-SCM method.

IV. CONCLUSIONS AND DISCUSSION

In this paper, we extended our investigations¹⁰ of energetics, conductance, and mesoscopic forces in a jellium modeled nanowire (sodium) using the local-density-functional-based shell correction method to variable-shaped wires, i.e., containing a constricted region modeled here by a parabolic dependence of the cross-sectional radii in the constriction on z (see Fig. 1). The results shown above, particularly the oscillations in the total energy of the wire as a function of the length of the variable-shaped constricted region (and correspondingly its narrowest width), the consequent oscillations in the elongation force, the corresponding discrete sequence of magic wire configurations, and the direct correlation between these oscillations and the stepwise quantized conductance of the nanowires, originate from quantization of the electronic states (i.e., formation of subbands) due to the reduced lateral (transverse) dimension of the nanowires. These results are in correspondence with our earlier LDA-SCM in-

vestigation of jellium-modeled uniform nanowires.¹⁰ Moreover, in the current study of a wire with a variable (adiabatic) shaped constriction, we found that the oscillatory behavior of the energetic and transport properties is governed by the subband quantization spectrum (termed here electronic shells) at the narrowest part of the constriction. This characteristic is supported and corroborated by our semiclassical analysis (Sec. III).

We reiterate here that such oscillatory behavior, as well as the appearance of ‘‘magic numbers’’ and ‘‘magic configurations’’ of enhanced stability, are a general characteristic of finite-size fermionic systems and are in direct analogy with those found in simple-metal clusters (as well as in ³He clusters²⁸ and atomic nuclei^{29,30}), where electronic shell effects on the energetics^{7,8,11,27} (and most recently shape dynamics⁵¹ of jellium modeled clusters driven by forces obtained from shell-corrected energetics) have been studied for over a decade.

While these calculations provide a useful and instructive framework, we remark that they are not a substitute for theories where the atomistic nature and specific atomic arrangements are included^{12–14,5,6} in evaluation of the energetics (and dynamics) of these systems (see in particular Refs. 5 and 6, where first-principles molecular-dynamics simulations of electronic spectra, geometrical structure, atomic dynamics, electronic transport, and fluctuations in sodium nanowires have been discussed).

Indeed, the atomistic structural characteristics of nanowires^{12–14} (including the occurrence of cluster-derived structures of particular geometries^{5,6}), which may be observed through the use of high-resolution microscopy,⁵² influence the electronic spectrum and transport characteristics, as well as the energetics of nanowires and their mechanical properties and response mechanisms. In particular, the me-

chanical response of materials involves structural changes through displacement and discrete rearrangement of the atoms. The mechanisms, pathways, and rates of such structural transformations are dependent on the arrangements and coordinations of atoms, the magnitude of structural transformation barriers, and the local shape of the wire, as well as possible dependency on the history of the material and the conditions of the experiment (i.e., fast versus slow extensions). Further evidence for the discrete atomistic nature of the structural transformations is provided by the shape of the force variations [compare the calculated Fig. 3(b) in Ref. 12 and Fig. 3 in Ref. 13 with the measurements shown in Figs. 1 and 2 in Ref. 20], and the interlayer spacing period of the force oscillations when the wire narrows. While such issues are not addressed by models that do not include the atomistic nature of the material, the mesoscopic (in a sense universal) phenomena described by our model are of interest, and may guide further research in the area of finite-size systems in the nanoscale regime. Such further investigations include the occurrence of magic configurations (i.e., sequences of enhanced stability specified by number of particles, size, thickness, or shape) in clusters, dots, wires, and thin films of normal, as well as superconducting, metals, and the effect of magnetic fields which can influence the energetics in such systems (e.g., leading to magnetostriction effects) through variations of the subband spectra, in analogy with magnetotransport phenomena in nanowires.³⁸

Several directions for improving the model (while remaining within a jellium framework) are possible. These include: (i) consideration of more complex shapes. For example, in our current model the elongation is distributed over the entire constriction throughout the process, while a more realistic description should include a gradual concentration of the elongation, and consequent shape variation, to the narrower part of the constriction as found through molecular-dynamics simulations;^{12,14} (ii) use of a stabilized-jellium description⁵³ of the energetics of the nanowire in order to give it certain elements of mechanical stability. In this context, note also that from the total energy shown in Fig. 4(c), and the corresponding total force [Fig. 5(c)], it is evident that in our current model, except for the region of large elongation close to the breaking point (i.e., $\Delta L/L_0 \geq 2.5$), the wire is unstable against spontaneous collapse (that is shortening), i.e., there are no energetic barriers against such a process, while both experiments²⁰ and MD simulations¹³ show that compression of such wires requires the application of an external force. Improvements of the model in these directions are most desirable in light of the aforementioned experimental²⁰ and MD simulations¹³ observations that the total oscillating forces for elongation and compression of nanowires are of opposite signs (i.e., negative and positive,

respectively), while our current (equilibrium model) is limited to certain aspects of the tensile part of an elongation-compression cycle; (iii) inclusion of bias voltage effects in calculations of the energetics and conductance of nanowires.^{39,54} While such effects may be expected to have little influence (particularly on the energetics) at small voltages, they could be of significance at larger ones. Work in these directions is in progress in our laboratory.

ACKNOWLEDGMENTS

This research was supported by a grant from the U.S. Department of Energy (Grant No. FG05-86ER45234) and the AFOSR. Useful comments by W.D. Luedtke are gratefully acknowledged. Calculations were performed at the Georgia Institute of Technology Center for Computational Materials Science.

APPENDIX

In this appendix, we discuss briefly a semiclassical treatment of temperature effects on the oscillatory behavior of the force and conductance in nanowires. The grand-canonical thermodynamic potential at finite temperature T is given by

$$\Omega = -k_B T \sum_i \ln \left[1 + \exp \left(\frac{\mu - \epsilon_i}{k_B T} \right) \right], \quad (\text{A1})$$

where i denotes (n, m, p_\perp) , and μ is the chemical potential.

From Eq. (A1), the finite temperature expressions for Ω^{osc} , F^{osc} , and G^{osc} differ from those given for the zero-temperature limit in Eqs. (33), (35), and (36), respectively, by a multiplicative factor in the sums of these equations. This factor is given by⁵⁵

$$\Psi(X_{MQ}) = \frac{X_{MQ}}{\sinh(X_{MQ})}, \quad (\text{A2a})$$

where

$$X_{MQ} = \frac{2\pi M k_B T a(0) \sin(\pi Q/M)}{\hbar v_F}, \quad (\text{A2b})$$

with v_F being the Fermi velocity. For $T=0$, $\Psi(x) = 1$.

Note that the temperature dependence given in Eq. (A2) is valid for systems with $k_F a(0) \geq 1$, and leads to reduction of the oscillation amplitudes when $2\pi M k_B T \geq \Delta \epsilon$, where $\Delta \epsilon = \hbar v_F / [a(0) \sin(\pi Q/M)]$ is an effective energy-level spacing of the electrons contributing to the oscillatory parts of the thermodynamic potential, force, and conductance.

¹See articles in *Large Clusters of Atoms and Molecules*, edited by T.P. Martin (Kluwer, Dordrecht, 1996).

²See articles in Proceedings of the 8th International Symposium on Small Particles and Inorganic Clusters, Copenhagen, 1996, edited by H.H. Anderson [Z. Phys. D **40**, 1–578 (1997)].

³See articles in *Atomic and Nanometer-Scale Modifications of Ma-*

terials: Fundamentals and Applications, edited by Ph. Avouris (Kluwer, Dordrecht, 1993).

⁴See articles in *Nanowires*, edited by P.A. Serena and N. Garcia (Kluwer, Dordrecht, 1997).

⁵U. Landman, R.N. Barnett, and W.D. Luedtke, Z. Phys. D **40**, 282 (1997).

- ⁶R.N. Barnett and U. Landman, *Nature (London)* **387**, 788 (1997).
- ⁷W.A. De Heer, *Rev. Mod. Phys.* **65**, 611 (1993).
- ⁸C. Yannouleas and U. Landman, in *Large Clusters of Atoms and Molecules* (Ref. 1), p. 131.
- ⁹T.P. Martin, *Phys. Rep.* **273**, 199 (1996).
- ¹⁰C. Yannouleas and U. Landman, *J. Phys. Chem. B* **101**, 5780 (1997).
- ¹¹C. Yannouleas and U. Landman, *Phys. Rev. B* **48**, 8376 (1993); *Chem. Phys. Lett.* **210**, 437 (1993).
- ¹²U. Landman, W.D. Luedtke, N. Burnham, and R.J. Colton, *Science* **248**, 454 (1990).
- ¹³U. Landman, W.D. Luedtke, B.E. Salisbury, and R.L. Whetten, *Phys. Rev. Lett.* **77**, 1362 (1996).
- ¹⁴U. Landman, W.D. Luedtke, and J. Gao, *Langmuir* **12**, 4514 (1996).
- ¹⁵E.N. Bogachek, A.M. Zagoskin, and I.O. Kulik, *Fiz. Nizk. Temp.* **16**, 1404 (1990) [*Sov. J. Low Temp. Phys.* **16**, 796 (1990)].
- ¹⁶J.I. Pascual, J. Mendez, J. Gomez-Herrero, J.M. Baro, N. Garcia, and V.T. Binh, *Phys. Rev. Lett.* **71**, 1852 (1993).
- ¹⁷L. Olesen, E. Laegsgaard, I. Stensgaard, F. Besenbacher, J. Schiøtz, P. Stoltze, K.W. Jacobsen, and J.N. Nørskov, *Phys. Rev. Lett.* **72**, 2251 (1994).
- ¹⁸J.I. Pascual, J. Mendez, J. Gomez-Herrero, J.M. Baro, N. Garcia, U. Landman, W.D. Luedtke, E.N. Bogachek, and H.-P. Cheng, *Science* **267**, 1793 (1995).
- ¹⁹D.P.E. Smith, *Science* **269**, 371 (1995).
- ²⁰G. Rubio, N. Agrait, and S. Vieira, *Phys. Rev. Lett.* **76**, 2302 (1996).
- ²¹A. Stalder and U. Durig, *Appl. Phys. Lett.* **68**, 637 (1996).
- ²²J.M. Krans, J.M. van Ruitenbeek, V.V. Fisun, I.K. Yanson, and L.J. de Jongh, *Nature (London)* **375**, 767 (1995).
- ²³J.L. Costa-Kramer, N. Garcia, P. Garcia-Mochales, and P.A. Serena, *Surf. Sci.* **342**, 11 144 (1995).
- ²⁴J.M. van Ruitenbeek, M.H. Devoret, D. Esteve, and C. Urbina, *Phys. Rev. B* **56**, 12 566 (1997). In this study, a uniform wire (i.e., with the cross section independent of the location on the symmetry axis) has been investigated. Electron-density spillout effects were approximated in an ad hoc manner.
- ²⁵C.A. Stafford, D. Baeriswyl, and J. Bürki, *Phys. Rev. Lett.* **79**, 2863 (1997). In this study, a wire of non-uniform shape has been studied using a free-electron model and assuming a constant bulk value of the wire's Fermi energy for all wire configurations. The last assumption implies neglect of the strong screening effects in metals as discussed in Ref. 24, where, within the context of a free-electron model, it is noted that this can lead to substantial deviations (that are largest for small cross sectional radii) of the electronic density from bulk values. We also note that the expression given in this paper for the surface energy is at variance (i.e., a factor of five too large) with the correct result for the infinite-barrier free-electron model given in Ref. 26 (see pp. 266–267; we thank Dr. N.D. Lang for pointing out this discrepancy). Reference 26 includes also a critical discussion pertaining to limitations of the free-electron model.
- ²⁶N.D. Lang, in *Solid State Physics*, edited by H. Ehrenreich, F. Seitz, and D. Turnbull (Academic Press, New York, 1973), Vol. 28, p. 225.
- ²⁷C. Yannouleas and U. Landman, *Phys. Rev. B* **51**, 1902 (1995); *Phys. Rev. Lett.* **78**, 1424 (1997); *J. Chem. Phys.* **107**, 1032 (1997).
- ²⁸C. Yannouleas and U. Landman, *J. Chem. Phys.* **105**, 8734 (1996); *Phys. Rev. B* **54**, 7690 (1996).
- ²⁹V.M. Strutinsky, *Nucl. Phys. A* **95**, 420 (1967); **122**, 1 (1968).
- ³⁰Å. Bohr and B.R. Mottelson, *Nuclear Structure*, Vol. II (Benjamin, Reading, MA, 1975).
- ³¹Here we use the Gunnarsson-Lundqvist xc functional [see O. Gunnarsson and B.I. Lundqvist, *Phys. Rev. B* **13**, 4274 (1976)].
- ³²C.H. Hodges, *Can. J. Phys.* **51**, 1428 (1973).
- ³³L.I. Glazman, G.B. Lesovik, D.E. Khmel'nitskii, and R.I. Shekhter, *Pis'ma Zh. Éksp. Teor. Fiz.* **48**, 218 (1988) [*JETP Lett.* **48**, 238 (1988)].
- ³⁴A. Yacoby and Y. Imry, *Phys. Rev. B* **41**, 5341 (1990).
- ³⁵C. Yannouleas and R.A. Broglia, *Phys. Rev. A* **44**, 5793 (1991); C. Yannouleas, R.A. Broglia, M. Brack, and P.-F. Bortignon, *Phys. Rev. Lett.* **63**, 255 (1989); M. Brack, *Phys. Rev. B* **39**, 3533 (1989); W. Ekardt, *ibid.* **29**, 1558 (1984).
- ³⁶R. Landauer, *Philos. Mag.* **21**, 863 (1970).
- ³⁷Y. Imry, in *Directions in Condensed Matter Physics*, edited by G. Grinstein and G. Mazenko (World Scientific, Singapore, 1986), p. 101.
- ³⁸E.N. Bogachek, A.G. Scherbakov, and U. Landman, *Phys. Rev. B* **53**, R13 246 (1996).
- ³⁹N.D. Lang, *Phys. Rev. B* **52**, 5335 (1995).
- ⁴⁰M. Brandbyge, K.W. Jacobsen, and J.K. Nørskov, *Phys. Rev. B* **55**, 2637 (1997).
- ⁴¹T.N. Todorov and A.P. Sutton, *Phys. Rev. Lett.* **70**, 2138 (1993).
- ⁴²J.B. Keller and S.I. Rubinow, *Ann. Phys. (N.Y.)* **9**, 24 (1960); in this context see also R. Landauer, Ph.D. thesis, Harvard University, 1950.
- ⁴³M. Brack and R.K. Bhaduri, *Semiclassical Physics* (Addison-Wesley, Reading, MA, 1997).
- ⁴⁴E. Jahnke, F. Emde, and F. Loesch, *Tables of Higher Functions* (McGraw-Hill, New York, 1960).
- ⁴⁵R.B. Dingle, *Proc. R. Soc. London, Ser. A* **212**, 47 (1952).
- ⁴⁶E.N. Bogachek and G.A. Gogadze, *Zh. Éksp. Teor. Fiz.* **63**, 1839 (1972) [*Sov. Phys. JETP* **36**, 973 (1973)].
- ⁴⁷A. Erdelyi, *Asymptotic Expansions* (Dover, New York, 1956).
- ⁴⁸E.N. Bogachek, M. Jonson, R.I. Shekhter, and T. Swahn, *Phys. Rev. B* **50**, 18 341 (1994); see in particular Eqs. (15) and (17), with $T_0 = 1$, $\alpha = 0$.
- ⁴⁹Yu. V. Sharvin, *Zh. Éksp. Teor. Fiz.* **48**, 984 (1965) [*Sov. Phys. JETP* **21**, 655 (1965)].
- ⁵⁰V.I. Falko and G.B. Lesovik, *Solid State Commun.* **84**, 835 (1992); J.A. Torres, J.I. Pascual, and J.J. Saenz, *Phys. Rev. B* **49**, 16 581 (1994); E.N. Bogachek, A.G. Scherbakov, and U. Landman, *Phys. Rev. B* **56**, 1065 (1997).
- ⁵¹C. Yannouleas and U. Landman, *J. Phys. Chem. A* (to be published).
- ⁵²T. Kizuka, K. Yamada, S. Deguchi, M. Naruse, and N. Tanaka, *Phys. Rev. B* **55**, R7398 (1997).
- ⁵³J.P. Perdew, H.Q. Tran, and E.D. Smith, *Phys. Rev. B* **42**, 11 627 (1990).
- ⁵⁴N.D. Lang, *Phys. Rev. B* **45**, 13 599 (1992); **49**, 2067 (1994).
- ⁵⁵Such functional dependence on the temperature of the amplitude of oscillations of thermodynamic and transport properties in metals is a typical one; see, e.g., A.A. Abrikosov, *Fundamentals of the Theory of Metals* (Elsevier, Amsterdam, 1988).